Layer-by-layer photonic crystal horn antenna

Andrew R. Weily,[1] Karu P. Esselle,[1] and Barry C. Sanders[2,3]
[1]*Department of Electronics, Macquarie University, Sydney, NSW, 2109, Australia*
[2]*Centre for Quantum Computer Technology, Macquarie University, Sydney, NSW, 2109, Australia*
[3]*Institute for Quantum Information Science, University of Calgary, Alberta, Canada T2N 1N4*
(Received 24 September 2003; revised manuscript received 4 May 2004; published 14 September 2004)

We introduce a horn antenna in a three-dimensional layer-by-layer photonic crystal that provides highly efficient transmission from a defect waveguide to free space. This device is physically realizable, thus providing a significant advance over an ideal two-dimensional photonic crystal horn antenna. Through numerical simulations we demonstrate the directional nature of the radiation pattern in the *H*-plane and its broader radiation characteristics in the *E*-plane. The antenna is shown to achieve a bandwidth that is almost equal to that of the defect waveguide, which illustrates that this horn antenna operates as an excellent output coupler for the photonic crystal waveguide. Further, the horn antenna may be easily integrated with other layer-by-layer photonic crystal components to form ultracompact devices for communication systems.

DOI: 10.1103/PhysRevE.70.037602 PACS number(s): 42.70.Qs, 42.82.Et, 41.20.Jb

Photonic crystal (PC) materials are extremely useful in the design of antennas. PC's are periodic dielectric and/or metallic structures that prevent the propagation of electromagnetic waves in one or more dimensions [1]. The band of frequencies for which this occurs is known as the photonic band gap (PBG). There have been several applications of PC's in the field of antennas: substrates for planar antennas [2], reflectors for dipole antennas [3,4], resonator antennas [5], and, more recently, two-dimensional photonic crystal horn and array antennas [6]. Each of these antennas has one thing in common; they exploit the properties of the PC to somehow shape the radiation characteristics of the device. The photonic crystal horn antenna (PCHA) also uses a defect PC waveguide to deliver energy to its radiating aperture. This gives it the advantage of being able to integrate the antenna with other signal processing components in the PC to create a single compact device, such as a photonic crystal array antenna (PCAA) [6]. We would like to point out that since completing our work on the PCHA, we discovered that another group had described a similar concept in an earlier patent [7] but gave few details on its actual implementation.

Although the PCHA and PCAA were able to successfully demonstrate these concepts, they have one drawback: they were modeled in a two-dimensional PC and therefore are not physically realizable. In this Brief Report, we remedy this situation by presenting an analysis of a horn antenna in a three-dimensional PC—the layer-by-layer photonic crystal horn antenna (LPCHA)—as shown in Fig. 1. This antenna configuration is physically realizable and retains all the advantages of the two-dimensional PCHA such as wide operating bandwidth, high directivity, and scalable operating frequency. However, due to its extra dimension the performance of the LPCHA cannot be easily extrapolated from the two-dimensional PCHA results. It requires a full three-dimensional numerical technique to model the additional electromagnetic confinement in the third dimension. This increases both the complexity of the numerical technique and the computational resources needed to achieve a design with desirable performance. In contrast to the two-dimensional PCHA, the three-dimensional wave guidance and radiation patterns of the LPCHA also enables the possibility of experimental verification.

In essence, the LPCHA is an adiabatic transition from a defect waveguide to free space, where the transition or taper of the defect waveguide is limited to a single plane of the

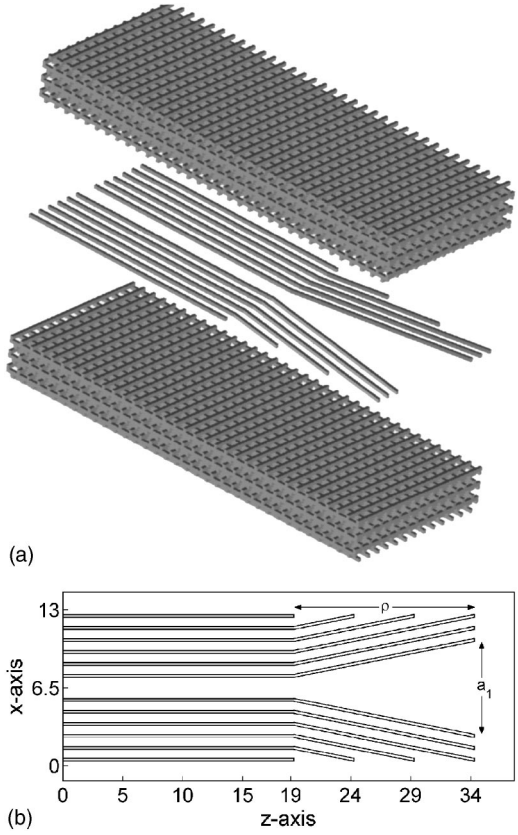

FIG. 1. (a) Exploded view of the *H*-plane LPCHA. Layer 13 contains the defect waveguide and splayed rods that form the horn antenna. (b) Layer 13 of the *H*-plane LPCHA viewed from above, and the computational domain used for its analysis. The units of each axis are given in lattice constants, *a*, to generalize the results presented. The electromagnetic source is placed at $x=6.5a$, $z=15a$.

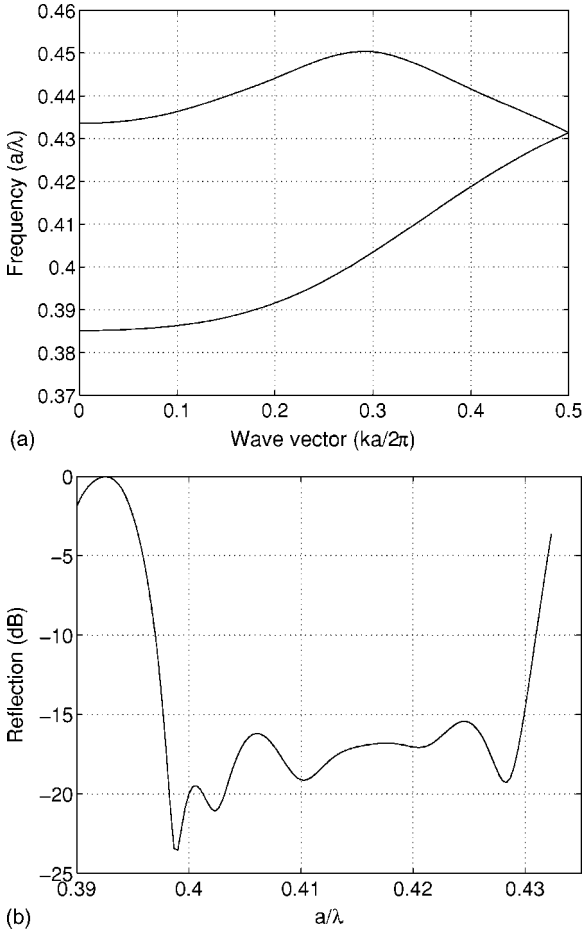

FIG. 2. (a) Dispersion diagram for the layer-by-layer photonic crystal defect waveguide calculated using a supercell with a size of $7\times7\times1$ lattice constants. (b) Computed reflection coefficient versus normalized frequency for the LPCHA with taper length $\rho=15a$ and aperture width $a_1=8a$.

device. This plane is known as the *H*-plane because it is parallel to the magnetic field of the free space mode. Here we consider the implementation for the specific case of a three-dimensional layer-by-layer PC; however, the concept can be extended to other structures as well. Though we do not implement the PCHA in any other PC's, the adiabatic transition numerically simulated for the layer-by-layer PC should work equally well for other three-dimensional PC structures, to create efficient and directive transitions to free space. Further, it can be implemented in either one or both planes of the defect waveguide.

The layer-by-layer, or woodpile, PC was chosen to implement the PCHA because of its wide, complete PBG [8]. Our implementation of the layer-by-layer PC used rods with a rectangular cross section, with a rod width of $0.25a$ and rod height of $0.3a$, where a is the lattice constant of the PC; the permittivity used for the rods was 11.56 to correspond with GaAs at optical frequencies. We calculated the PBG for the woodpile using a plane-wave expansion method implemented in RSOFT's BANDSOLVE™ software package. The PBG extends in normalized frequency from $a/\lambda=0.376$ to 0.455, or 19.0%.

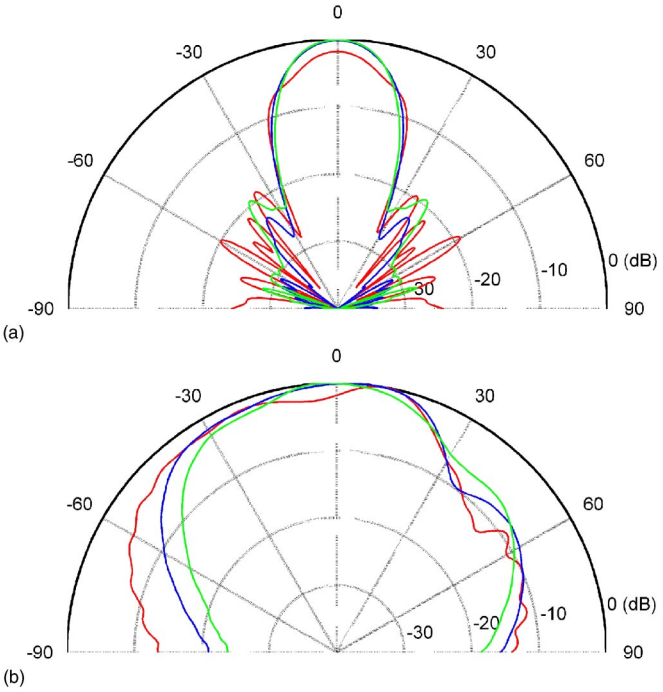

FIG. 3. (Color online) (a) *H*-plane and (b) *E*-plane radiation patterns for the LPCHA with a taper length of $\rho=15a$, aperture width of $a_1=8a$, and an aperture height of $b_1=0.3a$. The red line corresponds to $a/\lambda=0.397$, the blue line to $a/\lambda=0.414$, and the green line to $a/\lambda=0.427$. Angle 0° corresponds to the direction of the *z* axis.

We have numerically simulated the *H*-plane LPCHA in a 26 layer layer-by-layer PC structure using the FDTD method. The configuration of this device is depicted in the exploded view of Fig. 1. The defect waveguide is located on layer 13 of our device. This layer has been separated from the upper and lower crystals in the exploded view to show its details more clearly. It can be seen from this drawing that the rods have been splayed apart to form a horn antenna with a radiating aperture that is much wider than the defect waveguide. Since the plane of the taper is parallel to the magnetic field vector and the direction of maximum radiation, it is known as a *H*-plane LPCHA.

To show the details of the taper and the FDTD computational domain used to analyze the layer-by-layer PCHA, layer 13 of the device is also depicted in Fig. 1, as viewed from above. The antenna taper length is denoted as ρ, aperture width is labeled a_1. Though not shown in the figure, the aperture height is equal to the rod height and is $b_1=0.3a$. To terminate the feed waveguide section of the antenna a PC-based perfectly matched layer (PML) absorbing boundary condition with a length of $15a$ FDTD cells has been used [9]. The other five remaining boundaries used ten PML cells, since they are terminating free-space.

A defect waveguide in the layer-by-layer PC may be created by removing a single rod from the structure [10]. We have calculated the dispersion diagram for the layer-by-layer defect waveguide using the finite-difference time-domain (FDTD) method with periodic boundary conditions [11]. The discretization value used in our FDTD simulation was Δ

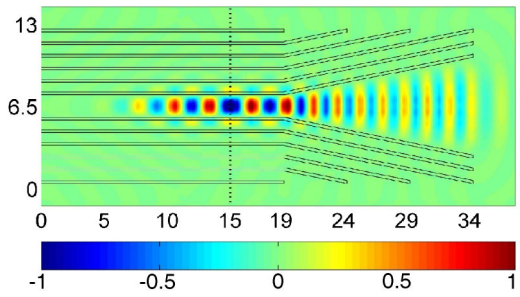

FIG. 4. (Color online) E_y field of the LPCHA at $a/\lambda=0.414$, taken as a horizontal slice through the center of layer 13 and plotted in linear scale. The fields have been normalized so that the maximum value is 1 and the minimum value is −1. The dotted vertical line at $z=15a$ shows the interface between the PC-based PML region and the PC defect waveguide. Note that the wave traveling to the left is absorbed by the PML.

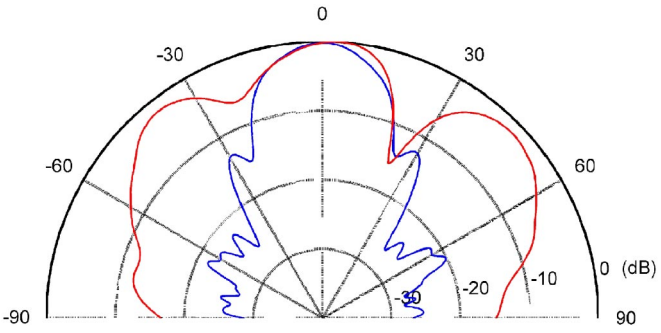

FIG. 5. (Color online) Radiation patterns for a layer-by-layer pyramidal PCHA at $a/\lambda=0.41$ with a taper length of $\rho=15a$, aperture width of $a_1=8a$, and an aperture height of $b_1=0.8a$. The blue line corresponds to the *H*-plane pattern and the red line to the *E*-plane.

$=a/16$ in the x and z directions, and $\Delta=a/13.3$ in the y direction.

The dispersion diagram calculated using this method for a supercell with a size of $7\times7\times1$ lattice constants is plotted in Fig. 2. This shows that the defect waveguide mode has a lower cutoff frequency of $a/\lambda=0.385$ when $ka/2\pi=0$. The frequency of the mode increases with wave number until it reaches $a/\lambda=0.431$ at $ka/2\pi=0.5$, which corresponds to the Brillouin zone boundary. Above this frequency the mode folds back, forming a second band that supports two modes for the frequency range of $a/\lambda=0.434$ to 0.450. We choose the operating range of the waveguide to be the region where it supports a single-mode and where the frequency increases approximately linearly with wave number. This range corresponds to $a/\lambda=0.390$ to 0.431; below $a/\lambda=0.390$ the wave number changes more rapidly with frequency.

In the analysis of the *H*-plane LPCHA our FDTD simulations used a discretization value of $\Delta=a/24$ in the x and z directions, and $\Delta=a/20$ in the z direction. The spectrum of the input pulse used to excite the antenna extended from $a/\lambda=0.390$ to 0.432. Using this pulse the reflection coefficient versus normalized frequency was calculated and is shown in Fig. 2. The −10 dB reflection coefficient bandwidth extends from $a/\lambda=0.397$ to 0.431, or 8.2%, for the configuration with $\rho=15a$ and $a_1=8a$. We choose −10 dB as our reference value to determine the bandwidth of the LPCHA because it corresponds to a reflected power level of less than or equal to 10% of the input power: at this level the layer-by-layer defect waveguide is well matched to free space.

To calculate the far-field radiation patterns of the antenna, a near-field to far-field transformation has been used in our FDTD code. *H*- and *E*-plane radiation patterns for $a/\lambda=0.397$, 0.414, and 0.427 are presented in Fig. 3 in polar form where the frequencies chosen correspond to the lower, center, and upper operating frequencies of the device. These plots show the directive nature of the antenna in the *H*-plane. In the *E*-plane the radiating aperture of the antenna is very narrow, so the radiation pattern is much broader, or less directive. At the lower operating frequency there is a slight shift in the direction of the maximum radiation to 10° in elevation; this is due to the slight asymmetry of the antenna in this plane as well as diffraction effects from the ends of the crystal. To illustrate the nature of the fields of the antenna, we give a linear scale plot for the field distribution at normalized frequency $a/\lambda=0.414$ in Fig. 4.

We have also analyzed the emission pattern for a pyriamidal horn antenna. In this device the taper exists in both the *E*- and *H*-planes to create a larger radiating aperture. The radiation patterns and dimensions of the antenna are given in Fig. 5. The *E*-plane pattern has become more directive than those of Fig. 3 due to the increased aperture height b_1 of the pyriamidal horn antenna.

In summary, we have theoretically demonstrated a transition from a defect waveguide in a three-dimensional PC to free space: the layer-by-layer photonic crystal horn antenna (LPCHA). The defect waveguide in the layer-by-layer PC is tapered in the *H*-planes of the antenna to give highly efficient, directional radiation. The −10 dB reflection coefficient bandwidth of the antenna is 8.2%, which is almost equal to the non-dispersive operating range of the defect waveguide defined earlier. The directional nature of the LPCHA, especially in the *H*-plane, has been shown through computed far-field radiation patterns for the device over its operating bandwidth. This makes it useful as an antenna or an array element at microwave, millimeter-wave, and optical frequencies.

This research was funded by an Australian Research Council (ARC) Discovery Grant. A.R.W. acknowledges financial support from a Macquarie University MURF Grant and an ARC Linkage APD (CSIRO) Grant. The authors thank the Australian Centre for Advanced Computing and Communications (AC3) for access to supercomputing facilities. B.C.S. acknowledges financial support from Alberta's informatics Circle of Research Excellence (iCORE) fund.

[1] J. D. Joannopoulos, R. D. Meade, and J. N. Winn, *Photonic Crystals: Molding the Flow of Light* (Princeton University Press, Princeton, NJ, 1995).
[2] E. R. Brown, C. D. Parker, and E. Yablonovitch, J. Opt. Soc. Am. B **10**, 404 (1993).
[3] M. P. Kesler, J. G. Maloney, and B. L. Shirley, Microwave Opt. Technol. Lett. **11**, 169 (1996).
[4] G. S. Smith, M. P. Kesler, and J. G. Maloney, Microwave Opt. Technol. Lett. **21**, 191 (1999).
[5] R. Biswas, E. Ozbay, B. Temelkuran, M. Bayindir, M. M. Sigalas, and K. M. Ho, J. Opt. Soc. Am. B **11**, 1684 (2001).
[6] A. R. Weily, K. P. Esselle, and B. C. Sanders, Phys. Rev. E **68**, 016609 (2003).
[7] R. L. Moore, M. P. Kesler, J. G. Maloney, and B. L. Shirley, US Patent 5,689,275, 1997.
[8] K. M. Ho, C. T. Chan, C. M. Soukoulis, R. Biswas, and M. M. Sigalas, Solid State Commun. **89**, 413 (1994).
[9] A. R. Weily, L. Horvath, K. P. Esselle, and B. C. Sanders, Microwave Opt. Technol. Lett. **40**, 1 (2004).
[10] A. Chutinan and S. Noda, Appl. Phys. Lett. **75**, 3739 (1999).
[11] A. Taflove and S. C. Hagness, *Computational Electrodynamics: The Finite-Difference Time-Domain Method*, 2nd ed. (Artech House, Boston, MA, 2000).